Delocalized Two-Exciton States in DNA Scaffolded Cyanine Dimers

Paul D. Cunningham[1,*], *Sebastián A. Díaz*[1], *Bernard Yurke*,[2] *Igor L. Medintz*[1], *and Joseph S. Melinger*[1,*]

[1]U.S. Naval Research Laboratory, Washington, DC 20375, United States

[2]Boise State University, Boise, Idaho 83725, United States

*paul.cunningham@nrl.navy.mil

*joseph.melinger@nrl.navy.mil

ABSTRACT

The engineering and manipulation of delocalized molecular exciton states is a key component for artificial biomimetic light harvesting complexes as well as alternative circuitry platforms based on exciton propagation. Here we examine the consequences of strong electronic coupling in cyanine homodimers on DNA duplex scaffolds. The most closely spaced dyes, attached to positions directly across the double-helix from one another, exhibit pronounced Davydov splitting due to strong electronic coupling. We demonstrate that the DNA scaffold is sufficiently robust to support observation of the transition from the lowest energy (J-like) one-exciton state to the non-local two-exciton state, where each cyanine dye is in the excited state. This transition proceeds via sequential photon absorption and persists for the lifetime of the exciton, establishing this as a controlled method for creating two-exciton states. Our observations suggest that DNA-organized dye networks have potential as platforms for molecular logic gates and entangled photon emission based on delocalized two-exciton states.

TOC Figure: 1.71" x 3"

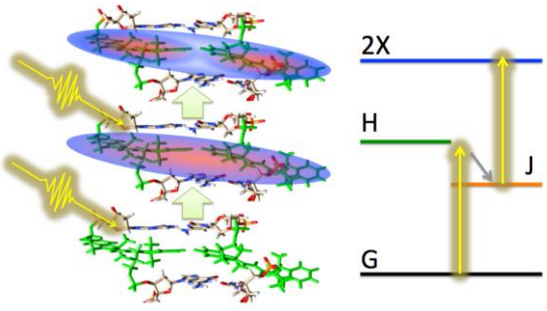

KEYWORDS: DNA scaffolds, molecular exciton, electron-vibration coupling, cyanine dyes, ultrafast spectroscopy

Delocalized molecular excitons are known to play a central role in optoelectronic applications such as light harvesting[1] and organic photovoltaics.[2] More recently, suitably constructed dye networks have been considered in the context of information processing systems in which excitons serve as the information carriers.[3-5] Analogous to the formation of molecular orbitals from linear combinations of atomic orbitals, molecular excitons form when strong coupling between transition dipoles cause individual exciton states on spatially separated chromophores to hybridize. The resulting delocalized excitons are spread in a wavelike manner over the interacting dyes. This process is well understood in molecular crystals and aggregates,[6] where it gives rise to a variety of optical phenomena including Davydov splitting,[7] quantum coherence,[8] exchange narrowing,[9] enhanced light-matter interactions,[10] superradiance,[11, 12] and other nonlinear optical phenomena.[13] While incoherent hopping of localized excitons, mediated by Förster resonance energy transfer (FRET), may become inefficient for a large number of individual steps, natural photosynthetic systems utilize strong electronic coupling and delocalized states to optimize efficient long-range energy transport.[14, 15] The high density of chromophores in such systems can exceed the component density of electronic circuitry such that excitonic logic structures[5, 16] have been proposed as a means for classical computing to keep pace with Moore's law. These properties and applications have led to growing interest in the purposeful and controlled design of delocalized exciton networks.

While biological systems rely on proteins to organize chromophore networks, controlling protein folding presents a roadblock to their use in artificial networks. DNA nanotechnology provides an alternative biomolecular scaffold for the rational and

predictable design of complex networks through programmable self-assembly. In particular, DNA scaffolds allow for fluorophores to be precisely arranged with sub-nm resolution, a capability that has been exploited to form light-harvesting antennae,[17-19] photonic wires,[20-23] biological sensors,[24, 25] nano-medicine,[26] molecular logic gates,[27-29] and nanoscale transducers.[30, 31] Typically, these systems have operated in the weak coupling limit where energy transport proceeds via FRET. Recently, several research groups have shown that it is possible to engineer strong electronic coupling in dye dimers[32-34], tetramers,[35] and templated aggregates[36-38] on DNA scaffolds through control of interdye separation. These systems show characteristic Davydov splitting and redistribution of oscillator strength typical of strong electron-vibrational (vibronic) coupling,[39] which is indicative of exciton delocalization. However, the phenomena typically associated with exciton delocalization in unscaffolded aggregates, such as quantum coherence oscillations[40] and biexciton formation[41], have not yet been reported for these systems.

Here, we report the creation of optically accessible two-exciton states in DNA scaffolded cyanine dimers through the formation of delocalized molecular excitons. Ultrafast transient absorption spectroscopy reveals optical transitions from the lowest (J-like) one-exciton to non-local two-exciton states. The long lifetimes of these transitions show that DNA-organized dye networks provide an opportunity to purposefully generate delocalized multi-exciton states. Such states could allow for the generation of entangled photon pairs[42] and may play an important role in molecular exciton circuitry.[5]

Cy3 and Cy5 homodimers were assembled on double-stranded (ds-) DNA wire scaffolds to allow precise control of the inter-dye separation. Cyanine dyes were selected for their high compatibility with fluorescent labeling of DNA, where the attachment chemistry is well established, the dyes show long term stability, and do not exhibit undesirable photoinduced charge transfer to the DNA nucleobases. Dye molecules were covalently attached to each of the DNA strands during synthesis through double phosphate attachment, which localize dyes and reduce the uncertainty in their position.[43, 44] The placement of one of the dyes in each homodimer was varied to produce dsDNA constructs where the interchromophore distance was either 1 bp or 0 bp separation; interchromophore distances ≥ 2 bp do not produce strong coupling.[34] Of particular interest was the 0 bp separation, which has recently been shown to produce the largest excitonic coupling for both Cy3 and Cy5 homodimers.[34, 35] The sequences for all cases are shown in the Supporting Information. DNA duplexes were formed by heating the complimentary strands to 90 ºC and then decreasing the temperature down to 4 ºC over the course of 1h. In addition to standard 2.5x PBS buffer solution (342.4 mM NaCl, 25 mM phosphate, and 6.75 mM KCl), cyanine homodimers were also prepared in 2:1 glycerol-H_2O containing 2.5X PBS, which yields an optical quality glass at cryogenic temperatures. In all cases solutions were prepared at ds-DNA concentrations of 4 μM.

Room temperature absorption spectra were recorded for 150 μL samples in a 1 cm path cuvette. Figures 1 a-b show absorption spectra of the 0 bp Cy3 and 0 bp Cy5 homodimers, which is similar to those that have been previously reported.[34, 35] In both cases, the 0 bp interchromophore separation leads to strong coupling with significant Davydov splitting of

the lowest energy absorption band with zero vibrational quanta (0-0) and increased oscillator strength of the higher energy vibrational progression (0-1 and 0-2). This redistribution of oscillator strength is a consequence of vibronic coupling and the hybridization of energy-levels.[45] Such vibronic coupling is thought to play an important role in producing long-lived quantum coherences in both biological and artificial systems.[40, 46, 47] In both systems, the lowest energy (J-like) transition is dominant, indicating a more end-on-end than oblique relative orientation of the chromophores. These general observations are relatively independent of buffer viscosity, since the absorption spectra are qualitatively similar for 0bp cyanine dimers at room temperature in PBS, 2:1 gly-H_2O/PBS (Gly), and cooled to approximately 100 K. We note that the absorption bands of both dimers redshift somewhat in Gly as compared to PBS. Low-temperature absorption spectra were measured on samples in a 1mm path cuvette mounted on the cold finger of a liquid nitrogen cryostat that was positioned in the sample arm of a spectrophotometer. While the cold finger reaches 77 K, in this geometry, the cuvette surface reaches only ~100 K. Linewidth narrowing due to reduced homogeneous broadening at 100 K reveals pronounced Davydov splitting, where the higher energy (H-like) and J-like states are clearly visible. The observed 0-0 splittings, estimated by Gaussian multipeak fits to the absorption spectra, are summarized in Table 1. The Davydov splittings are larger than the inhomogeneous linewidths of the absorption peaks and are a significant fraction of the dominant vibrational energy (~145 meV)[34] of the C-C stretch in the polymethine chain.[48] Such large splittings are consistent with the strong intermolecular coupling regime and the formation of molecular excitons.

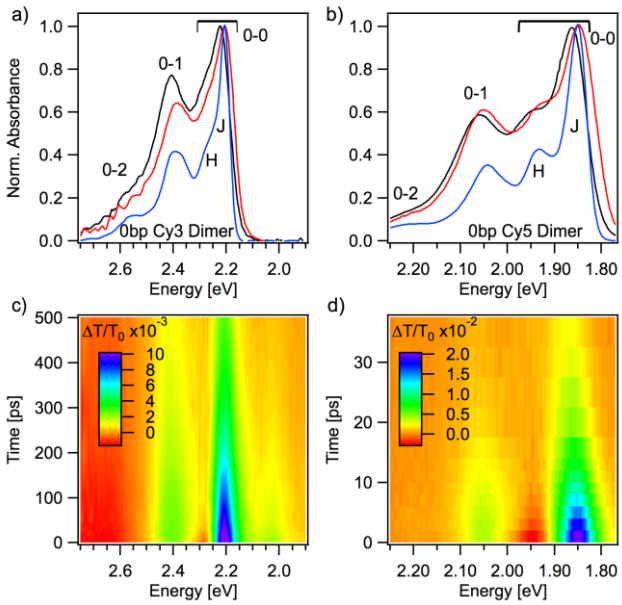

Figure 1. Cyanine Dimer Absorption and Transient Absorption Spectra. Normalized absorbance of the (a) 0 bp Cy3 dimer and (b) 0 bp Cy5 dimer in PBS at 295 K (black), 2:1 gly-H_2O/PBS at 295 K (red), and cooled to ~100K (blue). The 0-0, 0-1, and 0-2 vibronic bands are indicated, as are the H-like and J-like contributions to the 0-0 splitting. Transient absorption spectra measured at 295 K of the (c) 0 bp Cy3 dimer in PBS photoexcited at 2.26 eV (550 nm) and (d) 0 bp Cy5 dimer in PBS photoexcited at 1.86 eV (665 nm) show new excited state absorption near 2.26 eV (550 nm) and 1.94 eV (640 nm) respectively.

Table 1. Davydov Splitting of 0bp Cyanine Dimers

	0 bp Cy3 homodimer			0 bp Cy5 homodimer		
	PBS	Gly	100K	PBS	Gly	100K
0-0 Splitting meV	53 ± 2	66 ± 4	48 ± 1	85 ± 1	77 ± 4	73 ± 1
H-like peak meV (nm)	2264 (548)	2262 (548)	2252 (551)	1942 (639)	1917 (647)	1922 (645)
J-like peak meV (nm)	2211 (561)	2197 (565)	2204 (563)	1857 (668)	1840 (674)	1850 (670)

Ultrafast transient absorption (TA) spectroscopy was used to understand the excited state dynamics of the cyanine homodimers. The experimental apparatus, which has been described previously,[34] is based on a 1 kHz 800 nm 100 fs Ti:Sapphire laser that seeds an optical parametric amplifier for tunable excitation. A small amount of the 800 nm fundamental is used to generate the white light probe in a Sapphire plate, which is focused through the sample and analyzed with a scanning monochromator. Figures 1 c-d show TA spectra that are composed of a ground state bleach (GSB) and stimulated emission (SE) that resemble the absorption and emission spectra. Noticeably, a new excited state absorption (ESA) band is present in the 0 bp dimers that is absent from the monomer TA spectra, see Supporting Information. Similar spectra were observed for 0 bp cyanine dimers at room temperature in PBS, Gly, and at 100K, see Supporting Information for details. The ESA bands are approximately located at 2.26 eV (550 nm) and 1.94 eV (640 nm) for the 0 bp Cy3 homodimers and 0 bp Cy5 homodimer, respectively. Interestingly, these wavelengths approximately correspond to the H-like transitions for each dimer.

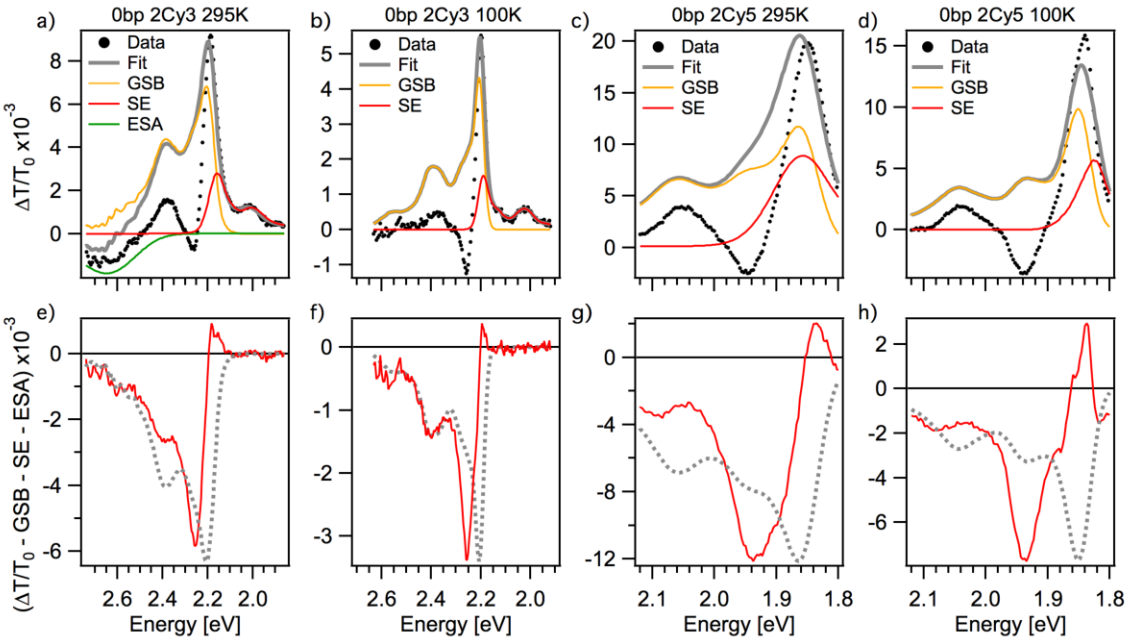

Figure 2. New Excited State Absorption Band in 0 bp Cyanine Dimers. Transient absorption spectra (black dots) of 0 bp Cy3 dimers in 2:1 gly-H_2O/PBS at (a) 295 K, and (b) cooled to ~100 K exhibit a new excited state absorption (ESA) band near 2.26 eV (550 nm). 0 bp Cy5 dimers in 2:1 gly-H_2O/PBS at (c) 295 K, and (d) cooled to ~100 K exhibit a similar new excited state absorption band near 1.94 eV (640 nm). Lines of best fit (grey) to the data are composed of estimated ground state bleach (orange), stimulated emission (red) and monomer S_1-S_n ESA (green). (e-h) The residuals (red) of the fits in (a-d) reveal the shape of the new ESA band. The dimer ground state absorbance curves (grey dashed) are included for comparison.

To extract the shape of the ESA bands from the TA spectra of the 0 bp cyanine homodimers, we can remove the overlapping contributions from the GSB and SE. This

technique has previously been used to identify ESA bands in molecular aggregates.[49] To obtain an estimate of the SE spectrum, the fluorescence spectrum is multiplied by λ^4.[50] For the Cy3 dimers, there is a second ESA near 2.64 eV (470 nm), which is also present in the Cy3 monomer,[34] and associated with S_1-S_n transitions. This known ESA band was also removed from the TA spectra to better estimate the shape of the unknown ESA band. Similarly shaped unknown ESA spectra are revealed thorough principle component analysis by applying singular value decomposition (not shown) to the TA spectra and keeping the leading eigenvalues. Figure 2 shows the new ESA band in both 0 bp cyanine homodimers found by the aforementioned subtractive method. The ESA bands resemble the ground-state absorption of the respective monomer, but are somewhat blue-shifted. This is the signature of a one-exciton to two-exciton transition.[41] Comparing the ESA band measured at 100K to the homodimer ground-state absorption band shows that the ESA peaks at the energy corresponding to the H-like transition energy. Therefore the ESA band corresponds to an optical transition from the one-exciton J-like band to a two-exciton level located at approximately twice the monomer energy. Interestingly, a vibrational progression is apparent in the extracted one-to-two exciton transition ESA spectra, consistent with the strong vibronic coupling present in these molecular dimers.

To better understand the nature of the new ESA bands, we can examine the Frenkel two-exciton Hamiltonian for a dimer.[6] The derivation below shows only the electronic interactions, which are sufficient for a qualitative understanding. The dimer system can be described by the following Frenkel exciton Hamiltonian

$$H = E_0\left(B_1^\dagger B_1 + B_2^\dagger B_2\right) + J\left(B_1^\dagger B_2 + B_2^\dagger B_1\right) + K\left(B_1^\dagger B_2^\dagger B_2 B_1\right) + \Delta\left(B_1^\dagger B_1^\dagger B_1 B_1 + B_2^\dagger B_2^\dagger B_2 B_2\right), \quad (1)$$

where, E_0 is the $S_0 \rightarrow S_1$ transition energy, J is the exciton exchange energy, K is the coupling between static dipole moments in S_1 and S_0,[51] and Δ is the local doubly-excited interaction energy defined as $\Delta = E_{S_0-S_N} - 2E_0$. The Δ term is sometimes referred to as the anharmonicity because it represents the deviation of the doubly-excited energy level from a harmonic ladder. We denote the ground state by $|0\rangle$. The one-exciton basis states are taken to be

$$|1\rangle = B_1^\dagger|0\rangle;\ |2\rangle = B_2^\dagger|0\rangle\,, \quad (2)$$

where the creation ($B_i^\dagger$) and annihilation (B_i) operators satisfy the Boson commutation relations:

$$\left[B_i, B_j^\dagger\right] = \delta_{ij} \quad (3)$$

$$\left[B_i, B_j\right] = 0 \quad (4)$$

In Eq. 2, $|1\rangle$ and $|2\rangle$ represent states where the excitation is on site 1 and 2 in the dimer, respectively. In the presence of the exchange interaction the one-exciton eigenenergies and eigenstates become

$$E_{1\pm} = E_0 \pm J \quad (5a)$$

$$|E_{1\pm}\rangle = \frac{1}{\sqrt{2}}(|1\rangle \pm |2\rangle). \quad (5b)$$

We use the symmetry-adapted states for the two-exciton basis as follows:

$$|S1\rangle = \frac{1}{2}\left(B_1^\dagger B_1^\dagger + B_2^\dagger B_2^\dagger\right)|0\rangle,\ |S2\rangle = B_1^\dagger B_2^\dagger|0\rangle, \quad (6a)$$

$$|A1\rangle = \frac{1}{2}\left(B_1^\dagger B_1^\dagger - B_2^\dagger B_2^\dagger\right)|0\rangle, \quad (6b)$$

where the *S* states are symmetric and the *A* state is antisymmetric. This leads to symmetric doubly-excited eigenenergies and eigenstates,

$$E_{2\pm} = \frac{4E_0+\Delta+K}{2} \pm \frac{1}{2}\sqrt{(\Delta-K)^2+16J^2} \tag{7a}$$

$$|E_{2+}\rangle = N[4J|S1\rangle + \left(K-\Delta+\sqrt{(K-\Delta)^2+16J^2}\right)|S2\rangle] \tag{7b}$$

$$|E_{2-}\rangle = N[(K-\Delta+\sqrt{(K-\Delta)^2+16J^2})|S1\rangle - 4J|S2\rangle] \tag{7c}$$

$$N = 1\Big/\sqrt{16J^2+(\Delta-K)+\sqrt{16J^2+(\Delta-K)^2}}, \tag{7d}$$

and an antisymmetric doubly-excited eigenenergy and eigenstate:

$$E_{2A} = 2E_0 + \Delta \tag{7e}$$

$$|E_{2A}\rangle = |A1\rangle. \tag{7f}$$

The dependence of the doubly-excited eigenenergies on the values of *J*, *K,* and Δ is shown in the Supporting Information. The doubly-excited manifold of a molecular dimer is composed of three states. The antisymmetric state is a local doubly-excited state that originates from an intramolecular transition and consists of a superposition between each single dye in the dimer being in the doubly-excited state. The symmetric states are of mixed local and non-local character, where the mixing ratio depends on Δ. The non-local contribution is that of a two-exciton state and involves one exciton on each dye in the dimer. For very large values of Δ, $|E_{2-}\rangle$ is purely non-local. In the 0 bp Cy3 dimers, we see from the S_1-S_N ESA band that the lowest local doubly-excited states have energy > 4.88 eV, such that Δ > 420 meV.

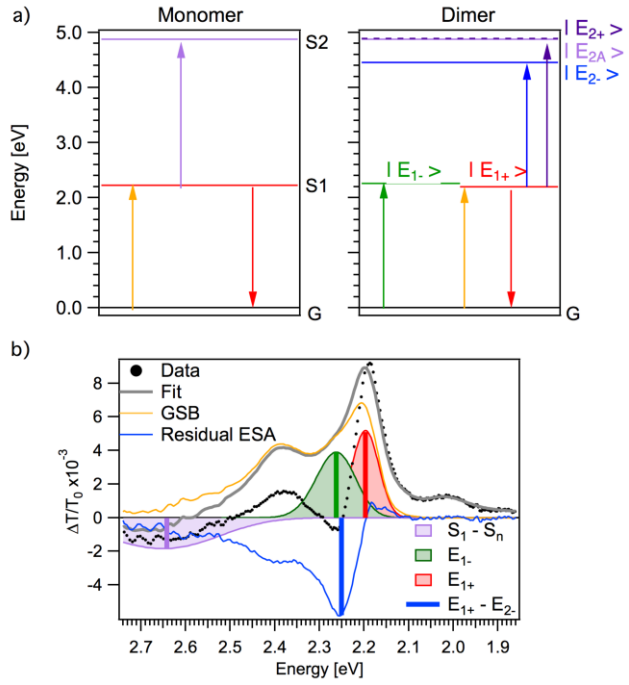

Figure 3. Vibronic Exciton Model of Cy3 Dimer Excited State Transitions. (a) Energy level structure for monomer (left) and electronically coupled dimers (right). The monomer consists of the ground state $|0\rangle$, and the first and nth excited electronic states. S_1 and S_N, respectively. The dimer consists of the ground state $|0\rangle$, singly-excited one-exciton manifold $|E_{1+}\rangle, |E_{1-}\rangle$, and the doubly-excited manifold $|E_{2-}\rangle, |E_{2A}\rangle, |E_{2+}\rangle$. The energetic ordering of the one-exciton manifold assumes J < 0, which is the case for a J-dimer. The orange and green arrows indicate impulsive excitation of $|E_{1+}\rangle$ and $|E_{1-}\rangle$, followed by rapid relaxation to the lowest one-exciton state. The upward blue and violet arrows indicate the allowed absorptive transitions from the singly-excited states to the doubly-excited states. The downward red arrow indicates stimulated emission. (b) Transient absorption spectra (black dots) of 0 bp Cy3 dimer in 2:1 gly-H_2O/PBS at 295 K, composed of ground state bleach (orange), stimulated emission, known S_1-S_n ESA (purple), and residual ESA (blue) from Figure 2. The $|E_{1+}\rangle$ (red) and $|E_{1-}\rangle$ (green) bands determined from multi-peak

Gaussian fits are indicated. The calculated electronic $|E_{1+}\rangle \rightarrow |E_{2-}\rangle$ transition energy for J = 33 meV, Δ = 420 meV, and K = 7 meV is indicated (blue vertical line).

Equations 5-7 result in the energy level diagram shown in Figure 3, which is relevant to discussing the transient absorption spectra of Cy3 and Cy5 dimers. The broadband ultrashort laser pulse simultaneously excites both $|E_{1-}\rangle$ (the H-like state) and $|E_{1+}\rangle$ (the J-like state), which is followed by rapid relaxation to $|E_{1+}\rangle$. The upward arrows indicate the absorptive singly-excited to doubly-excited transitions. The allowed transitions from $|E_{1+}\rangle$ are to the symmetric doubly-excited states: $|E_{1+}\rangle \rightarrow |E_{2-}\rangle$ and $|E_{1+}\rangle \rightarrow |E_{2+}\rangle$. The only allowed transition from the $|E_{1-}\rangle$ state is to the antisymmetric doubly-excited state: $|E_{1-}\rangle \rightarrow |E_{2A}\rangle$. The downward arrow indicates the stimulated emission transition from lower energy $|E_{1+}\rangle$ to the ground state.

We used the electronic coupling model, summarized in Equations 5-7, to simulate the transient absorption spectra for the Cy3 dimer 2:1 gly-H_2O/PBS at 295 K, Figure 3b. The Cy3 dimer was chosen because the TA spectra resolves both the GSB and SE, improving the accuracy of the calculated ESA band. First, we treat the single exciton states of the Cy3 dimer to fix the values of the coupling strength, J. Based on the Davydov splitting summarized in Table 1, we estimate J = 33 ± 2 meV for a monomer S1 energy of 2230 ± 3 meV (556 nm). From the location of the S_1-S_N ESA band in the Cy3 monomer TA spectra in Figure S2, we set as a lower bound Δ = 420 ± 50 meV. The ESA band transition $|E_{1+}\rangle \rightarrow |E_{2-}\rangle$ will occur at 2259 ± 4 meV (549 nm) for K = 7 ± 5 meV, which is an upper bound based on the value of Δ. This is consistent with the expected small permanent dipole

moment due to the mirror symmetry of the Cy3 molecule about the methine bridge. For these values of J, K, and Δ, the character of $|E_{2-}\rangle$ is largely $|S2\rangle$ (Figure S5), confirming that the observed ESA band is essentially a transition from the J-like one-exciton state to a non-local two-exciton state. We expect the Cy5 dimer to be qualitatively similar.

The appearance of the ESA band associated with the transition from one-exciton states to non-local two-exciton states depends strongly on the interchromophore spacing within the homodimer. Despite increased oscillator strength of the 0-1 shoulder of the ground state absorption due to strong vibronic coupling,[34] the Cy3 dimers placed on the DNA scaffold with a 1bp separation do not show this ESA band, see Supporting Information. In this case, the TA spectra closely resemble that previously reported for the monomer.[34, 44] One possible explanation is that the 1bp separation weakens the DNA by creating two neighboring sites without base-pairing, which allows for more DNA breathing near this site and in turn leads to a larger distribution of dye separations, orientations, and coupling strengths. An increase in disorder and a smaller average exchange coupling would allow only a small sub-ensemble to possess sufficient coupling strength to produce significant Davydov splitting and support the one-to-two exciton transition.

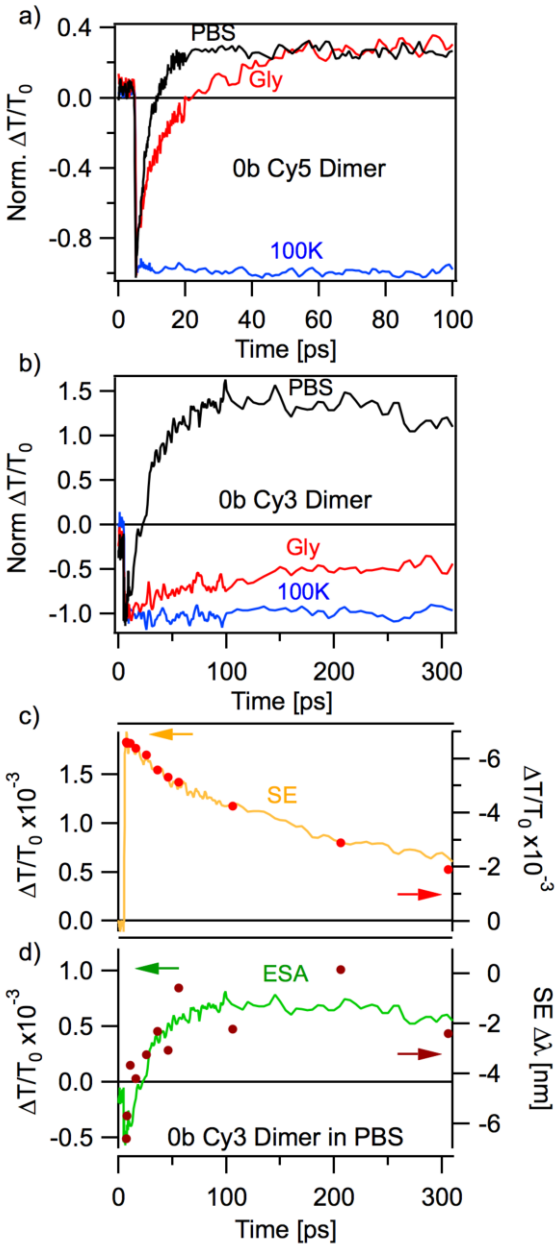

Figure 4. One-to-Two Exciton Dynamics in 0 bp Cyanine Dimers. (a) Dynamics measured at the excited state absorption (ESA) maximum for 0 bp Cy5 dimers in PBS (black), 2:1 gly-H_2O/PBS (red) and cooled to ~100K (blue). (b) Dynamics measured at the ESA maximum for 0 bp Cy3 dimers in PBS (black), 2:1 gly-H_2O/PBS (red) and cooled to ~100 K (blue). (c) Comparison between the ESA amplitude (red, dots) calculated from fits to the transient absorption (TA) spectra and the measured SE (orange) dynamics at 2.03eV

(612 nm) for 0 bp Cy3 dimers in PBS. (d) Comparison between the shift in stimulated emission (SE) wavelength (dark red, dots) calculated from fits to the TA spectra and the measured ESA (green) dynamics at 2.28 eV (543 nm) for 0 bp Cy3 dimers in PBS.

Figures 4 a-b show the dynamics of the transition from the one-exciton J-like band to this non-local two-exciton level in the 0 bp cyanine homodimers. As this ESA band persists for picoseconds to nanoseconds after photoexcitation it should not be thought of as two-photon absorption, which is a coherent process. Instead, this ESA band arises from sequential absorption: first a photon is absorbed from the pump followed, after some delay, by the absorption of a second photon from the probe. Figure 4 a-b shows that both 0 bp cyanine dimers exhibit a fast decay of the ESA band in PBS that becomes longer in Gly, and even longer at 100 K. This anomalous fast decay component appears to be faster than the SE decay, which is unexpected since the one-to-two exciton transition should occur with the lifetime of the J-like band. For the Cy3 homodimers, if TA spectra are fit with GSB and SE components while allowing the SE band to vary in center wavelength, the fit coefficients reveals a redshift of the SE band that matches the anomalous fast decay component of the ESA band; see Figure 4c. This apparent fast decay is therefore artificial and assigned to a dynamic Stokes shift associated with solvent reorganization,[52] which becomes slower with increased solvent viscosity. A similar analysis cannot be performed on the Cy5 homodimers because the 1-0 shoulder of the SE band is not resolved within our experimental bandwidth, which introduces significant uncertainty in the SE center

wavelength. Therefore, we cannot determine with certainty the cause of the fast ESA decay component in the 0 bp Cy5 homodimers. However, we expect that a similar redshift of the SE band also produces the artificial fast ESA decay in that system.

The controlled creation of biexcitons in molecular dimers on DNA scaffolds may provide a platform to realize molecular exciton transistors. Such structures have previously been proposed by exploiting FRET to and from a local doubly-excited, i.e. S_2, state that acts as the Gate.[5] A limitation of such a scheme is the short, typically sub-picosecond, lifetime of the S_2 state; two-exciton states can be longer lived. So to realize such an application, a key parameter to optimize is the lifetime of the two-exciton state. Recent work has shown that biexciton lifetimes in PIC j-aggregates (PIC is chemically similar to Cy3) have been limited by exciton-exciton annihilation (EEA) to a few picoseconds,[53] which may be sufficient for use in the molecular logic gates. Applications requiring photon emission from two-exciton states may well require suppression of EEA, perhaps through the use of H-like coupling,[54] or through the control of the local and non-local character of the doubly excited state.[55] As such, control of dye-dye coupling and orientation using DNA scaffolding may prove useful in realizing long lived biexcitons in molecular dimers suitable for use in molecular logic gates.

We have examined the optical transitions of Cy3 and Cy5 homodimers on dsDNA scaffolds. Closely spaced (placed < 2 bp apart on the DNA duplex) dyes exhibit exciton delocalization characterized by Davydov splitting and redistribution of oscillator strength

due to strong vibronic coupling. This strong coupling opens a new transition from the single-exciton to a non-local two-exciton state for the dimer. This transition proceeds via sequential photon absorption from the J-like molecular exciton to the non-local two-exciton state, which can be intentionally created at any point during the exciton lifetime. This transition also exhibits a vibrational progression, consistent with the strong vibronic coupling. Our observations establish DNA scaffolds as a controlled and programmable means of creating strongly coupled dyes that exhibit the novel optical properties of molecular aggregates. The controlled creation of biexcitons is a crucial step towards proposed classical[5] and quantum[56] logic structures based on biexcitons. The non-local nature of these biexcitons may allow the exciton-to-biexciton transition to be used as the ON state of the gate molecule in a recently proposed FRET-based universal logic gate set.[56] Such biexciton states may also support the emission of energy entangled photon states[42] owing to the deterministic relationship between the transition energies. As such, DNA dye networks show promise for applications in the field of molecular excitonics, where such delocalized states can be used to create molecular wires for excitonic circuitry or molecular logic gates for next generation computing platforms.

SUPPORTING INFORMATION

Details concerning the DNA sequences, separation-dependence of Cy3 dimer transient absorption spectra, buffer dependence of Cy3 dimer transient absorption spectra, buffer dependence of Cy5 dimer transient absorption spectra, and the vibronic two-exciton eigensystem. This material is available free of charge *via* the Internet at __.

ACKNOWLEDGMENT

P.C., S.D., I.M., and J.S. would like to acknowledge support from the Office of Naval Research (ONR) via the U.S. Naval Research Laboratory (NRL) Nanoscience Institute as well as by the Office of the Assistant Secretary of Defense for Research and Engineering (OSD R&E) via the Laboratory University Collaborative Initiative (LUCI) program in support of the Vannevar Bush Faculty Fellowship (VBFF) program. B.Y. would like to acknowledge support from the National Science Foundation INSPIRE program grant number 1648655.

REFERENCES

1. Scholes, G. D.; Fleming, G. R.; Olaya-Castro, A.; van Grondelle, R. Lessons from nature about solar light harvesting. *Nat. Chem.* **2011,** *3*, 763-774.
2. Bredas, J.-L.; Sargent, E. H.; Scholes, G. D. Photovoltaic concepts inspired by coherence effects in photosynthetic systems. *Nat. Mater.* **2017,** *16*, 35-44.
3. Childs, A. M.; Gosset, D.; Webb, Z. Universal Computation by Multiparticle Quantum Walk. *Science* **2013,** *339*, 791-794.
4. Yurke, B.; Kuang, W. Passive linear nanoscale optical and molecular electronics device synthesis from nanoparticles. *Phys. Rev. A* **2010,** *81*, 033814.
5. Sawaya, N. P. D.; Rappaport, N.; Tabor, D. P.; Aspuru-Guzik, A. Excitonics: A Set of Gates for Molecular Exciton Processing and Signaling. *ACS Nano* **2018,** *12*, 6410-6420.
6. Kasha, M.; Rawls, H. R.; El-Bayoami, M. A. The molecular exciton model in molecular spectroscopy. *Pure Appl. Chem.* **1965,** *11*, 371-392.
7. Davydov, A. V. The Theory of Molecular Excitons. *Soviet Phys* **1964,** *7*, 145-178.
8. Lim, J.; Palecek, D.; Caycedo-Soler, F.; Lincoln, C. N.; Prior, J.; von Berlepsch, H.; Huelga, S. F.; Plenio, M. B.; Zigmantas, D.; Hauer, J. Vibronic origin of long-lived coherence in an artificial molecular light harvester. *Nat. Commun.* **2015,** *6*, 7755.
9. Knapp, E. W. Lineshapes of Molecular Aggregates - Exchange Narrowing and Intersite Correlation. *Chem. Phys.* **1984,** *85*, 73-82.
10. Vasa, P.; Wang, W.; Pomraenke, R.; Lammers, M.; Maiuri, M.; Manzoni, C.; Cerullo, G.; Lienau, C. Real-time observation of ultrafast Rabi oscillations between excitons and plasmons in metal nanostructures with J-aggregates. *Nat. Photonics* **2013,** *7*, 128-132.
11. Spano, F. C.; Kuklinski, J. R.; Mukamel, S. Temperature- Dependent Superradiant Decay of Excitons in Small Aggregates. *Phys. Rev. Lett.* **1990,** *65*, 211-214.

12. Fidder, H.; Knoester, J.; Wiersma, D. A. Superradiant emission and optical dephasing in J-aggregates. *Chem. Phys. Lett.* **1990,** *171*, 529-536.
13. Spano, F. C.; Mukamel, S. Cooperative nonlinear optical response of molecular aggregates: Crossover to bulk behavior. *Phys. Rev. Lett.* **1991,** *66*, 1197-1200.
14. Strümpfer, J.; Sener, M.; Schulten, K. How Quantum Coherence Assists Photosynthetic Light Harvesting. *J. Phys. Chem. Lett.* **2012,** *3*, 536-542.
15. Romero, E.; Novoderezhkin, V. I.; van Grondelle, R. Quantum design of photosynthesis for bio-inspired solar-energy conversion. *Nature* **2017,** *543*, 355-365.
16. Pistol, C.; Dwyer, C.; Lebeck, A. R. Nanoscale optical computing using resonance energy transfer logic. *IEEE Micro.* **2008,** *28,* 7-19.
17. Woller, J. G.; Hannestad, J. K.; Albinsson, B. Self-Assembled Nanoscale DNA-Porphyrin Complex for Artificial Light Harvesting. *J. Amer. Chem. Soc.* **2013,** *135*, 2759-2768.
18. Buckhout-White, S.; Spillmann, C. M.; Algar, W. R.; Khachatrian, A.; Melinger, J. S.; Goldman, E. R.; Ancona, M. G.; Medintz, I. L. Assembling programmable FRET-based photonic networks using designer DNA scaffolds. *Nat. Commun.* **2014,** *5*, 5615.
19. Dutta, P. K.; Levenberg, S.; Loskutov, A.; Jun, D.; Saer, R.; Beatty, J. T.; Lin, S.; Liu, Y.; Woodbury, N. W.; Yan, H. A DNA-Directed Light-Harvesting/Reaction Center System. *J. Amer. Chem. Soc.* **2014,** *136*, 16618-16625.
20. Heilemann, M.; Tinnefeld, P.; Mosteiro, G. S.; Parajo, M. G.; van Hulst, N. F.; Sauer, M. Multistep Energy Transfer in Single Molecular Photonic Wires. *J. Amer. Chem. Soc.* **2004,** *126*, 6514-6515.
21. Klein, W. P.; Diaz, S. A.; Buckhout-White, S.; Melinger, J. S.; Cunningham, P. D.; Goldman, E. R.; Ancona, M. G.; Kuang, W.; Medintz, I. L. Utilizing HomoFRET to Extend DNA-Scaffolded Photonic Networks and Increase Light-Harvesting Capability. *Adv. Opt. Mater.* **2017**, *6*, 1700679.
22. Nicoli, F.; Barth, A.; Bae, W.; Neukirchinger, F.; Crevenna, A. H.; Lamb, D. C.; Liedl, T. Directional Photonic Wire Mediated by Homo-Förster Resonance Energy Transfer on a DNA Origami Platform. *ACS Nano* **2017,** *11*, 11264-11272.
23. Kownacki, M.; Langenegger, S. M.; Liu, S. X.; Häner, R. Integrating DNA Photonic Wires into Light-Harvesting Supramolecular Polymers. *Angew. Chem. Int. Ed.* **2019,** *58*, 751-755.
24. Algar, W. R.; Khachatrian, A.; Melinger, J. S.; Huston, A. L.; Stewart, M. H.; Susumu, K.; Blanco-Canosa, J. B.; Oh, E.; Dawson, P. E.; Medintz, I. L. Concurrent Modulation of Quantum Dot Photoluminescence Using a Combination of Charge Transfer and Förster Resonance Energy Transfer: Competitive Quenching and Multiplexed Biosensing Modality. *J. Amer. Chem. Soc.* **2017,** *139*, 363-372.
25. Vietz, C.; Schütte, M. L.; Wei, Q.; Richter, L.; Lalkens, B.; Ozcan, A.; Tinnefeld, P.; Acuna, G. P. Benchmarking Smartphone Fluorescence-Based Microscopy with DNA Origami Nanobeads: Reducing the Gap toward Single-Molecule Sensitivity. *ACS Omega* **2019,** *4*, 637-642.
26. Ma, W.; Zhan, y.; Zhang, Y.; Shao, X.; Xie, X.; Mao, C.; Cui, W.; Li, Q.; Shi, J.; Li, J.; Fan, C.; Lin, Y. An Intelligent DNA Nanorobot with in Vitro Enhanced Protein Lysosomal Degradation of HER2. *Nano Lett.* **2019,** *19*, 4505-4517.

27. Cannon, B. L.; Kellis, D. L.; Davis, P. H.; Lee, J.; Kuang, W.; Hughes, W. L.; Graugnard, E.; Yurke, B.; Knowlton, W. B. Excitonic AND Logic Gates on DNA Brick Nanobreadboards. *ACS Photonics* **2015,** *2*, 398-404.
28. Buckhout-White, S.; Brown III, C. W.; Hastman Jr, D. A.; Ancona, M.; Melinger, J. S.; Goldman, E. R.; Medintz, I. L. Expanding molecular logic capabilities in DNA-scaffolded multiFRET triads. *RSC Adv.* **2016,** *6*, 97587-97598.
29. Kellis, D. L.; Sarter, C.; Cannon, B. L.; Davis, P. H.; Graugnard, E.; Lee, J.; Pensack, R. D.; Kolmar, T.; Jäschke, A.; Yurke, B.; Knowlton, W. B. An All-Optical Excitonic Switch Operated in the Liquid and Solid Phases. *ACS Nano* **2019,** *13*, 2986-2994.
30. Bui, H.; Brown III, C. W.; Buckhout-White, S.; Diaz, S. A.; Stewart, M. H.; Susumu, K.; Oh, E.; Ancona, M. G.; Goldman, E. R.; Medintz, I. L. Transducing Protease Activity into DNA Output for Developing Smart Bionanosensors. *Small* **2019,** *15*, 1805384.
31. Ma, R.; Kellner, A. V.; Ma, V. P.-Y.; Su, H.; Deal, B. R.; Brockman, J. M.; Salaita, K. DNA probes that store mechanical information reveal transient piconewton forces applied by T cells. *Proc. Nat. Acad. Sci. USA* **2019,** *116*, 16949-16954.
32. Nicoli, F.; Roos, M. K.; Hemmig, E. A.; Di Antonia, M.; de Vivie-Riedle, R.; Liedl, T. Proximity-Induced H-Aggregation of Cyanine Dyes on DNA-Duplexes. *J. Phys. Chem. A* **2016,** *120*, 9941-9947.
33. Kringle, L.; Sawaya, N. P. D.; Widom, J.; Adams, C.; Raymer, M. G.; Aspuru-Guzik, A.; Marcus, A. H. Temperature-dependent conformations of exciton-coupled Cy3 dimers in double- stranded DNA. *J. Chem. Phys.* **2018,** *148*, 085101.
34. Cunningham, P. D.; Kim, Y. C.; Diaz, S. A.; Buckhout-White, S.; Mathur, D.; Medintz, I. L.; Melinger, J. S. Optical Properties of Vibronically Coupled Cy3 Dimers on DNA Scaffolds. *J. Phys. Chem. B* **2018,** *122*, 5020-5029.
35. Cannon, B. L.; Kellis, D. L.; Patten, L. K.; Davis, P. H.; Lee, J.; Graugnard, E.; Yurke, B.; Knowlton, W. B. Coherent Exciton Delocalization in a Two-State DNA-Templated Dye Aggregate System. *J. Phys. Chem. A* **2017**, *121*, 6905-6916.
36. Winiger, C. B.; Langenegger, S. M.; Calzaferri, G.; Häner, R. Formation of Two Homo‐chromophoric H‐Aggregates in DNA‐Assembled Alternating Dye Stacks. *Angew. Chem. Int. Ed.* **2015,** *54*, 3643-3647.
37. Boulais, E.; Sawaya, N. P. D.; Veneziano, R.; Andreoni, A.; Banal, J. L.; Kundo, T.; Mandal, S.; Lin, S.; Schlau-Cohen, G. S.; Woodbury, N. W.; Yan, H.; Aspuru-Guzik, A.; Bathe, M. Programmed coherent coupling in a synthetic DNA-based excitonic circuit. *Nat. Mater.* **2018**, *17*, 159-166.
38. Zhou, X.; Mandal, S.; Jiang, S.; Lin, S.; Yang, J.; Liu, Y.; Whitten, D. G.; Woodbury, N. W.; Yan, H. Efficient Long-Range, Directional Energy Transfer through DNA-Templated Dye Aggregates. *J. Amer. Chem. Soc.* **2019,** *141*, 8473-8481.
39. Kühn, O.; Renger, T.; May, V. Theory of Exciton-Vibrational Dynamics in Molecular Dimers. *Chem. Phys.* **1996,** *204*, 99-114.
40. Halpin, A.; Johnson, P. J. M.; Tempelaar, R.; Murphy, R. S.; Knoester, J.; Jansen, T. L. C.; Miller, R. J. D. Two-dimensional spectroscopy of a molecular dimer unveils the effects of vibronic coupling on exciton coherences. *Nat. Chem.* **2014,** *6*, 196-201.
41. Fidder, H.; Knoester, J.; Wiersma, D. A. Observation of the one-exciton to two-exciton transition in a J aggregate. *J. Chem. Phys.* **1993,** *98*, 6564-6566.

42. Stevenson, R. M.; Young, R. J.; Atkinson, P.; Cooper, K.; Ritchie, D. A.; Shields, A. J. A semiconductor source of triggered entangled photon pairs. *Nature* **2006,** *439*, 179-182.
43. Stennett, E. M. S.; Ma, N.; van der Vaart, A.; Levitus, M. Photophysical and Dynamical Properties of Doubly Linked Cy3-DNA constructs. *J. Phys. Chem. B* **2014,** *118*, 152-163.
44. Cunningham, P. D.; Khachatrian, A.; Buckhout-White, S.; Deschamps, J. R.; Goldman, E. R.; Medintz, I. L.; Melinger, J. S. Ultrafast energy transfer in DNA wires with restricted dye motion. *J. Phys. Chem. B* **2014,** *188*, 14555-14565.
45. Polyutov, S.; Kühn, O.; Pullerits, T. Exciton-vibrational coupling in molecular aggregates: Electronic versus vibronic dimer. *Chem. Phys.* **2012,** *394*, 21-28.
46. Fuller, F. D.; Pan, J.; Gelzinis, A.; Butkus, V.; Senlik, S. S.; Wilcox, D. E.; Yocum, C. F.; Valkunas, L.; Abramavicius, D.; Ogilvie, J. P. Vibronic coherence in oxygenic photosynthesis. *Nat. Chem.* **2014,** *6*, 704-711.
47. Wang, L.; Griffin, G. B.; Zhang, A.; Zhai, F.; Williams, N. E.; Jordan, R. F.; Engel, G. S. Controlling quantum-beating signals in 2D electronic spectra by packing synthetic heterodimers on single-walled carbon nanotubes. *Nat. Chem.* **2017,** *9*, 219-225.
48. Mustroph, H.; Reiner, K.; Mistol, J.; Ernst, S.; Keil, D.; Hennig, L. Relationship between the Molecular Structure of Cyanine Dyes and the Vibrational Fine Structure of their Electronic Absorption Spectra. *Chem. Phys. Chem.* **2009,** *10*, 835-840.
49. Marciniak, H.; Li, X.-Q.; Würthner, F.; Lochbrunner, S. One-Dimensional Exciton Diffusion in Perylene Bisimide Aggregates. *J. Phys. Chem. A* **2010,** *115*, 648-654.
50. Deshpande, A. V.; Beindoun, A.; Penzkofer, A.; Wagenblast, G. Absorption and emission spectroscopic investigation of cyanovinyldiethylaniline dye vapors. *Chem. Phys.* **1990,** *142*, 123-131.
51. Abramavicius, D.; Palmieri, B.; Mukamel, S. Extracting Single and Two-Exciton Couplings in Photosynthetic Complexes by Coherent Two-Dimensional Electronic Spectra. *Chem. Phys.* **2008,** *357*, 79-84.
52. Petkov, B. K.; Gellen, T. A.; Farfan, C. A.; Carbery, W. P.; Hetzler, B. E.; Trauner, D.; Li, X.; Glover, W. J.; Ulness, D. J.; Turner, D. B. Two-Dimensional Electronic Spectroscopy Reveals the Spectral Dynamicsof Förster Resonance Energy Transfer. *Chem.* **2019,** *5*, 1-15.
53. Ma, F. Dynamics and Coherent Control of Exciton−Exciton Annihilation in Aqueous J‐Aggregate. *J. Phys. Chem. B* **2018,** *122*, 10746-10753.
54. Tempelaar, R.; Jansen, T. L. C.; Knoester, J. Exciton−Exciton Annihilation Is Coherently Suppressed in H‐Aggregates, but Not in J‐Aggregates. *J. Phys. Chem. Lett.* **2017,** *8*, 6113-6117.
55. Yan, Y.-a.; Kühn, O. Laser control of dissipative two-exciton dynamics in molecular aggregates. *New J. Phys.* **2012,** *14*, 105004.
56. Li, X.; Wu, Y.; Steel, D.; Gammon, D.; Stievater, T. H.; Katzer, D. S.; Park, D.; Piermarocchi, C.; Sham, L. J. An All-Optical Quantum Gate in a Semiconductor Quantum Dot. *Science* **2003,** *301*, 809-811.